Constrained 2-D/3-D Registration for Motion Compensation in AFib Ablation Procedures

Alexander Brost[1**], Andreas Wimmer[1], Rui Liao[2], Joachim Hornegger[1], and Norbert Strobel[3]

[1] Pattern Recognition Lab, Friedrich-Alexander-University Erlangen-Nuremberg, Erlangen, Germany,
[2] Siemens Corporate Research, Imaging and Visualization, Princeton, NJ, USA,
[3] Siemens AG, Healthcare, Forchheim, Germany.

Abstract. Fluoroscopic overlay images rendered from pre-operative volumetric data can provide additional guidance for physicians during catheter ablation procedures for treatment of atrial fibrillation (AFib). As these overlay images are compromised by cardiac and respiratory motion, motion compensation methods have been proposed. The approaches so far either require simultaneous biplane imaging for 3-D motion compensation or, in case of mono-plane X-ray imaging, provide only a limited 2-D functionality. To overcome the downsides of the previously suggested methods, we propose a new approach that facilitates full 3-D motion compensation even if only mono-plane X-ray views are available. To this end, we use constrained model-based 2-D/3-D registration to track a circumferential mapping catheter which is commonly used during AFib catheter ablation procedures. Our approach yields an average 2-D tracking error of 0.6 mm and an average 3-D tracking error of 2.1 mm.

1 Introduction

Atrial fibrillation (AFib), which is the most common arrhythmia, leads to an increased risk of stroke for the patient [1]. After the first treatment approaches using radio-frequency ablations by Haïssaguerre et al. [2], this method has now become an accepted treatment option [3]. Catheter ablation procedures are performed in electrophysiology (EP) labs usually equipped with modern C-arm X-ray systems. These devices often provide 3-D imaging of the heart [4] to overcome the issue that soft-tissue of the heard is difficult to see in X-ray images. Electro-anatomic mapping systems have been proposed in the past to show the catheter position in 3-D within a registered pre-operative data set [5,6,7,8]. While they promise to save X-ray dose, they add effort and cost to the procedure. In addition, mapping systems are virtual reality systems. They do not allow to instantly confirm catheter positions under X-ray with respect to detailed 3-D cardiac anatomy. In some instances, they may even be off with respect to the underlying anatomy [9]. Augmented fluoroscopy, using either CT, MRI or C-arm

** Alexander.Brost@informatik.uni-erlangen.de

CT, overlaying a pre-operative data set onto live fluoroscopic images can facilitate more precise catheter navigation and also reduce fluoroscopy time [10,11,12]. Unfortunately, catheter navigation under augmented fluoroscopy is compromised by cardiac and respiratory motion. A first approach to overcome this problem by providing a motion compensated overlay has been proposed in [13]. It involved tracking of commonly used circumferential mapping catheters. As atrial fibrillation (Afib) therapy takes place in the vicinity of the circumferential mapping catheter, catheter tracking can be assumed to capture the motion of the relevant treatment region correctly if the device has been firmly positioned. Fortunately, we can count on the physicians to provide us with a stable wall contact, as it is in their best interest. Otherwise complete isolation of the pulmonary veins (PVs) may fail due to undetected residual PV-atrial electrical connections. The intial proposed method generates a 3-D model of the catheter and applies an unconstrained 2-D/3-D registration to register the catheter model to biplane fluoroscopy images. In the first approach, a filter-based technique using a vessel enhancement filtering was used. The method was later extended by integrating a learning-based catheter segmentation [14]. However, this technique still required simultaneous biplane imaging. An approach for monoplane fluoroscopic imaging was introduced in [15] considering only a 2-D catheter and moving the overlay. That is, the projection of the pre-operative 3-D data set is shifted on the live fluoroscopic images in sync with the cardiac and respiratory motion. The last method might be the approach of choice if only a monoplane C-arm system is available. In EP labs equipped with biplane C-arm systems, often only one imaging plane is used at a time to reduce the dose to the patient. In this case, the methods suggested in [13,14] are not applicable. The 2-D method described in [15] is not ideal either, as it requires re-initialization of the catheter model as soon as the C-arm view direction changes. To improve the mono-plane situation, we propose a constrained 2-D/3-D registration to perform motion compensation using a 3-D catheter model. The generation of a 3-D catheter model requires only a single biplane shot. This way, the increase of X-ray radiation to the patient is kept to a minimum.

2 Three-Dimensional Catheter Model

In the first step of our method, a 3-D model of the circumferential mapping catheter is generated, as proposed in [13,16,14]. A single biplane frame is required to manually initialize the model generation step. Therefore, 2-D points $\boldsymbol{p}_\mathrm{A}, \boldsymbol{p}_\mathrm{B} \in \mathbb{R}^2$ are selected on the elliptically shaped part of the catheter in each imaging plane. The imaging planes are denoted by A and B. Two-dimensional ellipses $\boldsymbol{C}_\mathrm{A}, \boldsymbol{C}_\mathrm{B} \in \mathbb{R}^{3\times3}$ are then fitted to these points. These matrices fulfill the following equations

$$\boldsymbol{p}_\mathrm{A}^T \boldsymbol{C}_\mathrm{A} \boldsymbol{p}_\mathrm{A} = 0 \tag{1}$$

$$\boldsymbol{p}_\mathrm{B}^T \boldsymbol{C}_\mathrm{B} \boldsymbol{p}_\mathrm{B} = 0. \tag{2}$$

Two 3-D cones $\boldsymbol{Q}_\mathrm{A}, \boldsymbol{Q}_\mathrm{B} \in \mathbb{R}^{4\times4}$ are then computed by using the projection matrices $\boldsymbol{P}_\mathrm{A}, \boldsymbol{P}_\mathrm{B} \in \mathbb{R}^{3\times4}$

$$\boldsymbol{Q}_\mathrm{A} = \boldsymbol{P}_\mathrm{A}^T \boldsymbol{C}_\mathrm{A} \boldsymbol{P}_\mathrm{A} \tag{3}$$

$$\boldsymbol{Q}_\mathrm{B} = \boldsymbol{P}_\mathrm{B}^T \boldsymbol{C}_\mathrm{B} \boldsymbol{P}_\mathrm{B}. \tag{4}$$

These two 3-D cones are defined by the position of the X-ray tube relative to the projection of the elliptical catheter onto the imaging plane. The 3-D catheter model is computed by intersecting the two elliptical cones $\boldsymbol{Q}_A$ and $\boldsymbol{Q}_B$ corresponding to plane A and plane B of a biplane system respectively [17]. The solution is found by calculating η such that the quadric

$$\boldsymbol{Q}(\eta) = \boldsymbol{Q}_A + \eta \boldsymbol{Q}_B \tag{5}$$

is of rank 2 [17]. As pointed out in [13], there are two possible solutions. Prior knowledge about the pseudo-circular shape of the mapping catheter is used and the result that is more circular is chosen. The simulation results in [16] verify this assumption. The 3-D model is denoted as $\boldsymbol{m}_i \in \boldsymbol{R}^4$ in homogeneous coordinates as $\boldsymbol{m}_i = (m_{i,x}, m_{i,y}, m_{i,z}, 1)^T \in \mathbb{R}^4$ with $i \in [1, N]$ and N the number of model points. This step is performed only once.

3 Catheter Segmentation

In the second step of our method, we segment the catheter in the fluoroscopic images. To this end, we first crop the image around the region of interest which is a 400×400 pixels region around the projected center of the catheter model. In the first frame, the position is know from the initialization step, in all subsequent frames, the tracking result from the previous frame is used. The next step is catheter segmentation, which will be explained shortly. After segmentation, the resulting image is thinned [18]. To obtain a smooth image for registration, the distance transform for the skeletonized image is calculated [19]. The image processing steps are summarized in Fig. 1.

The catheter segmentation method has to fulfill two requirements. First, it has to be reliable. Second, it has to be fast. Speed is necessary to ensure that the catheter can be tracked in real-time at the frame rate required by the physician. In our case, a combination of Haar-like features and a cascade of boosted classifiers can meet both demands. Haar-like features [20] calculate various patterns of intensity differences. Some features detect edges, whereas others focus on line-like structures which are useful for detecting the catheter, as it is a thin object. Several feature prototypes are listed in Fig. 2(a). Actual features are obtained by shifting and scaling the prototypes within a predefined window. Thereby, contextual information around the center pixel is considered, which is important to differentiate between catheter and background structures. These features can be calculated efficiently through integral images.

Even for moderate window sizes, the resulting number of features is large and easily amounts to several hundreds of thousands. In order to achieve reliable and fast segmentation, the most suitable features for discriminating between

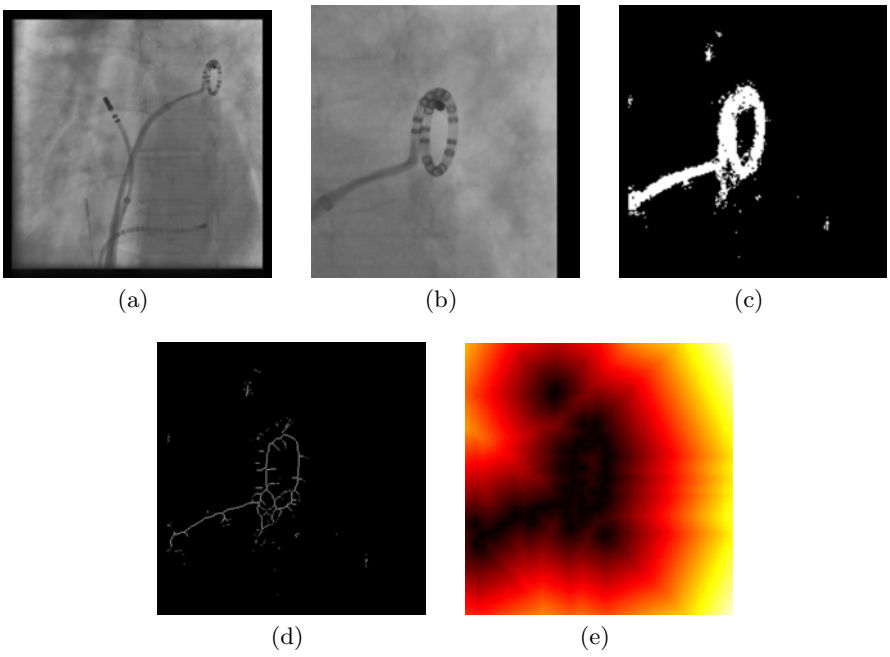

Fig. 1. (a) The original fluoroscopic input image. (b) Cropped image around the region-of-interest. (c) Segmentation using a boosted classifier cascade. (d) Skeletonized image. (e) Distance transformed image $\boldsymbol{I}_{\mathrm{DT}}$ to get a smooth image for registration.

catheter and background have to be chosen and integrated into a classifier in a suitable manner. This is carried out by the AdaBoost algorithm [21]. The idea is to combine several weak classifiers, which only have to be sligthly better than chance, to form a strong classifier. In the simplest case, a weak classifier amounts to a single feature and threshold. Weak classifiers are repeatedly evaluated on samples of a training set where the catheter has been annotated. The classifier minimizing the classification error is added to a linear combination of weak classifiers until the overall error is below the desired threshold. After each iteration, the importance of individual samples is re-weighted to put more emphasis on mis-classifications for the next evaluation.

Instead of single features and intensity thresholds, we use classification and regression trees (CARTs) [22] as weak classifiers. A CART is a small tree of fixed size. At each node, a threshold is associated with a feature partitioning the feature space. An example of a CART is shown in Fig. 2(b). Through this decomposition, flexibility is increased and objects with complex feature distributions can be handled.

Weighted combinations of CARTs are organized into a cascade, which is illustrated in Fig. 2(c). At each stage, a sample is either rejected or passed on to the next stage. Only if the sample is accepted at the final stage, it is assumed to

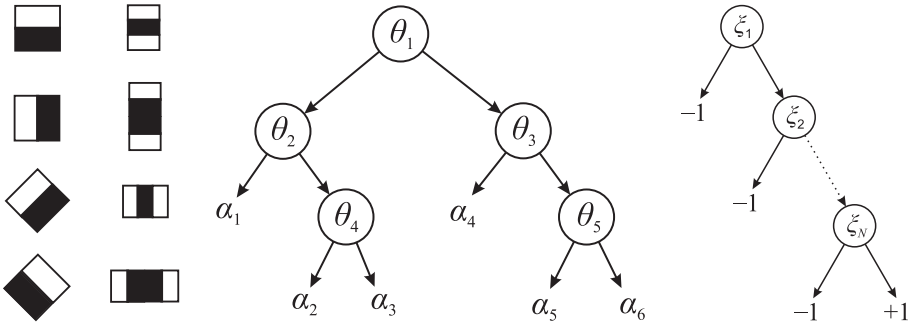

(a) Feature Types (b) Classification and Regression Tree (CART) (c) Cascade

Fig. 2. Features types and classifier structure for catheter segmentation: (a) several (lowpass) Haar filter examples used for feature extraction; (b) example of classification and regression tree (CART) with five feature nodes $\theta_1, \ldots, \theta_5$ and six leaves $\alpha_1, \ldots, \alpha_6$; (c) classifier cascade consisting of N stages with strong classifiers $\xi_1, \ldots \xi_N$. Each strong classifier ξ_i consists of a linear combination of weak classifiers, here CARTs.

belong to the object. Thus, during training, the focus is on maintaining a high true positive rate while successively reducing the false positive rate, either by adding more weak classifiers to a stage or by adding an entirely new stage. For training, a gold-standard segmentation of the catheter was used.

4 Constrained Model-Based 2-D/3-D Registration

In the third step of our method, the actual motion compensation is performed by a constrained model-based 2-D/3-D registration. The catheter model is manually initialized in the first pair of frames of a biplane sequence and afterwards tracked throughout the remainder of one monoplane sequence. Tracking itself is performed by rigid 2-D/3-D registration. The constraint used for registration is that the search range is restricted to all directions parallel to the imaging plane. No search is performed perpendicular to the optical plane, i.e., along the optical axis. This is not a major issue, because shifts along the optical axis merely result in size changes of the motion-compensated fluoroscopic overlay. A motion analysis of the LA, performed by Ector et al. [23], revealed that the dominant motion is in anterior-posterior and superior-inferior direction. They found that the degree of rotation is much less, and they contributed it to the deformation of the left atrium. The mismatch in depth between the 3-D overlay and the live fluoroscopic images mainly results in small changes of the LA size which we found negligible for augmented fluoroscopy applications in clinical practice. Therefore, we focused on the remaining dominant motion directions in superior-inferior and lateral directions. To carry out this constrained 2-D/3-D registration, the viewing direction $\boldsymbol{n} \in \mathbb{R}^3$ with $||\boldsymbol{n}||_2 = 1$ is obtained from the projection matrix

$\boldsymbol{P} \in \mathbb{R}^{3\times4}$. The viewing direction is perpendicular to all vectors that are parallel to the imaging plane. To calculate two spanning vectors of such a plane, an arbitrary vector $\boldsymbol{w} \in \boldsymbol{R}^3$ with $||\boldsymbol{w}||_2 = 1$ and $\boldsymbol{n}^T\boldsymbol{w} \neq 0$ is chosen. The spanning vectors $\boldsymbol{u}, \boldsymbol{v} \in \mathbb{R}^3$ of the search plane are then computed by

$$\boldsymbol{u} = \boldsymbol{n} \times \boldsymbol{w} \tag{6}$$

$$\boldsymbol{v} = \boldsymbol{n} \times \boldsymbol{u} \tag{7}$$

with $||\boldsymbol{u}||_2 = 1$ and $||\boldsymbol{v}||_2 = 1$. Depending on the choice of $\boldsymbol{w}$, the vectors $\boldsymbol{u}$ and $\boldsymbol{v}$ are different, but since these vectors span the same plane, any point on that plane can be represented by a linear combination of these two vectors. Moving a point $\boldsymbol{q} \in \mathbb{R}^3$ parallel to the imaging plane is achieved by

$$\boldsymbol{q}^\star = \boldsymbol{q} + \lambda\boldsymbol{u} + \mu\boldsymbol{v} \tag{8}$$

with the translated point $\boldsymbol{q}^\star \in \boldsymbol{R}^3$ and the amount of translation defined by $\lambda, \mu \in \mathbb{R}$.

We compute a transformation matrix $\boldsymbol{T}(\lambda, \mu) \in \boldsymbol{R}^{4\times4}$ as

$$\boldsymbol{T}(\lambda,\mu) = \begin{pmatrix} 1 & 0 & 0 & \lambda u_x + \mu v_x \\ 0 & 1 & 0 & \lambda u_y + \mu v_y \\ 0 & 0 & 1 & \lambda u_z + \mu v_z \\ 0 & 0 & 0 & 1 \end{pmatrix} \tag{9}$$

with $\boldsymbol{u} = (u_x, u_y, u_z)^T$ and $\boldsymbol{v} = (v_x, v_y, v_z)^T$. The objective function for the constrained registration is then defined by using the values of the distance transformed image $\boldsymbol{I}_{\mathrm{DT}}$ as cost function by

$$\hat{\lambda}, \hat{\mu} = \arg\min_{\lambda,\mu} \sum_i \boldsymbol{I}_{\mathrm{DT}} \left(\boldsymbol{P} \cdot \boldsymbol{T}(\lambda,\mu) \cdot \boldsymbol{m}_i \right). \tag{10}$$

Rotation is not considered, as we are primarily interested in the compensation of breathing motion which occurs in axial direction. The projection matrix considered for projecting the model into the imaging plane is not required to be one of the projection matrices used for model generation, i.e., the C-arm can be moved in between model generation and tracking. Given the parameters $\hat{\lambda}, \hat{\mu}$, found by a nearest-neighbor search, that minimize Eq. (10), the catheter model can be updated to $\boldsymbol{m}_i^\star \in \boldsymbol{R}^4$ by

$$\forall i : \boldsymbol{m}_i^\star = \boldsymbol{T}(\lambda,\mu) \cdot \boldsymbol{m}_i. \tag{11}$$

The same transformation $\boldsymbol{T}(\hat{\lambda}, \hat{\mu})$ is then also applied to the 3-D volumetric data set that is used for the image overlay. This way, we can achieve a 3-D motion compensation for mono-plane fluoroscopic images.

5 Evaluation and Results

Evaluation was performed using a leave-one-out validation approach. The tracking accuracy was measured in comparison to a gold-standard segmentation. The

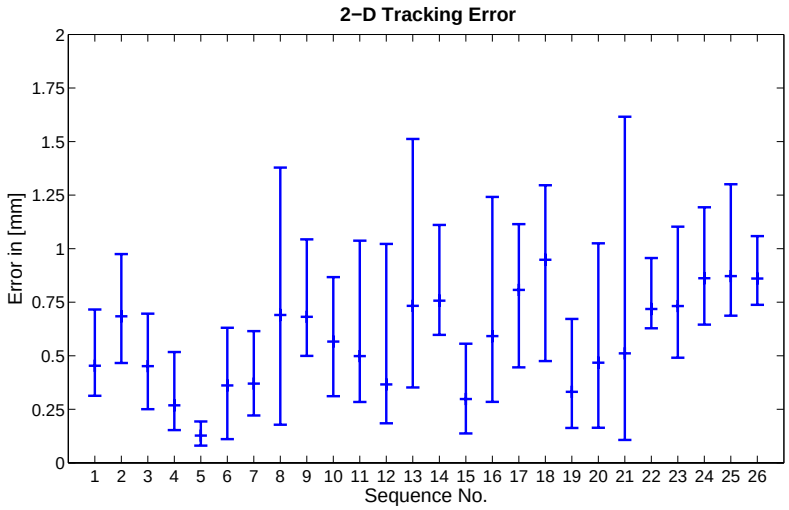

Fig. 3. Two-dimensional tracking error for all 26 sequences. For each sequence, the average error, minimum error, and maximum error is given. An overall mean error of 0.58 mm, an overall minimum error of 0.08 mm, and an overall maximum error of 1.62 mm was achieved.

sequence considered for testing was not included in the respective training data set. For evaluation, 13 clinical biplane sequences were available. Our data was taken from six different patients at one clinical site. They were recorded on an AXIOM Artis dBC biplane C-arm system (Siemens AG, Healthcare, Forchheim, Germany). For each sequence, a 3-D model was generated as described in Sec. 2. Afterwards, our method was evaluated by considering each imaging plane of the biplane sequences independently. This way, we obtained 26 sequences with a total frame number of 938 frames to evaluate catheter tracking. A 2-D tracking error was obtained by calculating the average 2-D distance of the projected catheter model to the gold-standard segmentation used for training. The average error, minimum error, and maximum error for each sequence are illustrated in Fig. 3. Our method yielded an overall mean error of 0.58 mm, an overall minimum error of 0.08 mm, and an overall maximum error of 1.62 mm.

Since the motion compensation is performed in 3-D, a 3-D error can estimated as well. To this end, the tip of circumferential mapping catheter was manually localized in 3-D using triangulation from two views. The available 3-D trajectories of the catheter tip were taken as a gold-standard for the observed 3-D motion.

In one sequence, the 3-D error turned out rather high, because the catheter moved significantly perpendicular to the optical plane, see Fig. 4. However, in cases where the circumferential mapping catheter was firmly placed at a pulmonary vein no such movement occurred, and we were able move the overlay well in sync with the 3-D motion. The method in [16] is still superior regarding

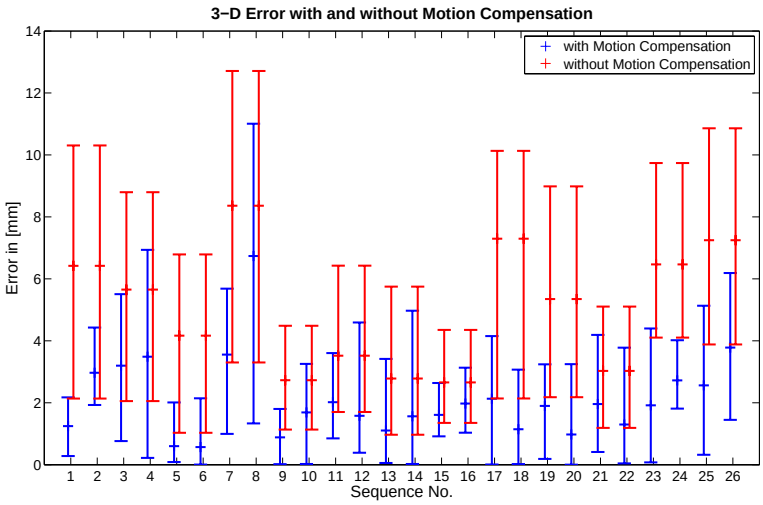

Fig. 4. Three-dimensional tracking error for all 26 sequences in comparison to the observed 3-D motion. For each sequence, the average, minimum, and maximum for the tracking error as well as the observed motion is given. On average, we observed an overall mean error of 2.12 mm, an overall minimum error of 0.01 mm, and an overall maximum error of 11.01 mm was achieved.

the 3-D error, but its better accuracy comes at the cost of simultaneous biplane fluorosopy, i.e., increased X-ray dose.

6 Discussion and Conclusions

The 2-D tracking error of our proposed method is in the same range as 2-D reference method [15]. But instead of performing only a 2-D/2-D registration, we now rely on a constrained 2-D/3-D registration involving a 3-D catheter model. The advantage of a 3-D catheter model is that re-positioning of the C-arm is possible whereas a 2-D catheter representation needs to be re-initialized if view directions change. Nevertheless, a pure 2-D approach is the method of choice if only a monoplane fluoroscopic system is available. In addition, our new approach is learning-based whereas the approach in [15] is filter-based. Therefore, our new method requires a training phase for the segmentation of the catheter. Note, however, that by using a learning-based method we might be able to improve the tracking results. At least, this is what we observed for the biplane approach [14]. Here, the filter-based approach [16] yielded a 2-D tracking error of 1.0 mm and a 3-D tracking error of 0.8 mm. Using a learning-based method, the errors were reduced to 0.8 mm in 2-D and to 0.7 mm in 3-D [14].

The dedicated biplane method [14] yields a smaller 3-D error than our new method, but it requires simultaneously biplane fluoroscopy. A comparison of all

Method Comparison			
	Our	**[14]**	**[15]**
Catheter Model	3-D	3-D	2-D
Compensation in	3-D	3-D	2-D
mono-/biplane fluoro	+/+	-/+	+/-
Mean 2-D Error:	0.58 mm	0.8 mm	0.59 mm
Mean 3-D Error:	2.12 mm	0.7 mm	—

Table 1. Comparison between available methods for respiratory and cardiac motion compensation during atrial fibrillation catheter ablation procedures. Our method uses a learning-based approach to segment a commonly used circumferential mapping catheter and then performs a mono-plane 2-D/3-D registration of a 3-D model to the segmentation. The method in [14] a bi-plane 2-D/3-D registration. The method in [15] uses a filter-based method to segment the same catheter and uses only a 2-D model which is registered to mono-plane sequences.

three methods (current approach, [14], [15]) is given in Tab. 1. In our current technique, we provide only a limited 3-D motion compensation but do not require simultaneously biplane fluoroscopy as in [14]. The limitation of our method is mainly related to the fact that motion along the viewing direction cannot be taken into account as depth information is hard to determine from mono-plane projection images. To achieve a depth correction, a perfect segmentation of the catheter would be required and, in addition, we would also need to know the exact dimensions of the catheter in 3-D, i.e., its diameter and its thickness. Any noise in the 2-D segmentation or at the 3-D model would decrease the accuracy of the depth estimate. To avoid this problem we have chosen to use only search directions parallel to the imaging plane. As a price to pay, we accept that the 3-D error will not be as good as in [15]. As in the previously presented methods, our new approach does not require a perfect segmentation of the circumferential mapping catheter, because the registration method can compensate for segmentation errors.

For comparison, electro-anatomic mapping systems provide a mean tracking error of 0.7 mm [24] which is comparable to our mean tracking error of 0.58 mm. In addition, our reference catheter, the circumferential mapping catheter, is directly at the site of ablation. Hence, it enables motion compensation for respiratory and cardiac motion without the need to separate these two motion patterns or the requirement to synchronize with ECG. Since we do not need to record the ECG signal, a stand-alone version of an augmented-reality, motion-compensated fluoroscopy system is possible.

A comparison between a frame with and without motion compensation is presented in Fig. 5. In a clinical setup, a physician working on a biplane system is likely to use his imaging planes in an alternating way. For such a clinical use case, our newly proposed method provides a significant advantage over the previously introduced methods [13,15] in terms of accuracy and practicality.

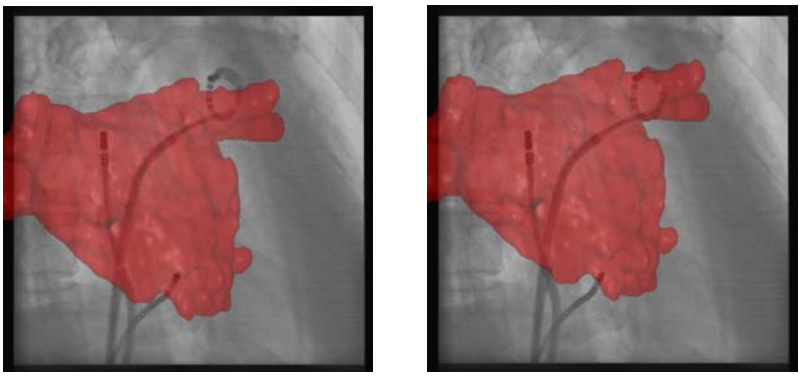

(a) (b)

Fig. 5. A comparison showing the difference if motion compensation is considered or not. (a) One frame of sequence 17 without motion compensation. (b) Shows the same frame of sequence 17 as in (a) but this time with motion compensation.

Acknowledgements

This work has been supported by the German Federal Ministry of Education and Research in the context of the initiative Spitzencluster Medical Valley - Europäische Metropolregion Nürnberg. Additional funding was provided by Siemens Healthcare.

References

1. Gage, B., Waterman, A., Shannon, W., Boechler, M., Rich, M., Radford, M.: Validation of Clinical Classification Schemes for Predicting Stroke. JAMA **285**(22) (June 13 2001) 2864–2870
2. Haissaguerre, M., Gencel, L., Fischer, B., Le Metayer, P., Poquet, F., Marcus, F., Clementy, J.: Successful Catheter Ablation of Atrial Fibrillation. J Cardiovasc Electrophysiol **5** (1994) 1045–1052
3. Calkins, H., Brugada, J., Packer, D., Cappato, R., Chen, S., Crijns, H., Damiano, R., Davies, D., Haines, D., Haissaguerre, M., Iesaka, Y., Jackman, W., Jais, P., Kottkamp, H., Kuck, K., Lindsay, B., Marchlinski, F., McCarthy, P., Mont, J., Moradi, F., Nademanee, K., Natale, A., Pappone, C., Prystowsky, E., Raviele, A., Ruskin, J., Shemin, R.: HRS/EHRA/ECAS Expert Consensus Statement on Catheter and Surgical Ablation of Atrial Fibrillation: Recommendations for Personnel, Policy, Procedures and Follow-Up. Europace **9**(6) (June 2007) 335–379
4. Prümmer, M., Wigström, L., Hornegger, J., Boese, J., Lauritsch, G., Strobel, N., Fahrig, R.: Cardiac C-arm CT: Efficient Motion Correction for 4D-FBP. In: IEEE Nuclear Science Symposium Conference Record. (2006)
5. Wittkampf, F., Wever, E., Derksen, R., Wilde, A., Ramanna, H., Hauer, R., Robles de Medina, E.: LocaLisa - New Technique for Real-Time 3-Dimensional Localization of Regular Intracardiac Electrodes. Circulation **99**(13) (1999) 1312–1317

6. Kistler, P., Rajappan, K., Jahngir, M., Earley, M., Harris, S., Abrams, D., Gupta, D., Liew, R., Ellis, S., Sporton, S., Schilling, R.: The Impact of CT Image Integration into an Electroanatomic Mapping System on Clinical Outcomes of Catheter Ablation of Atrial Fibrillation. Journal of Cardiovascular Electrophysiology **17**(10) (October 2006) 1093–1101
7. Kistler, P.M., Earley, M.J., Harris, S., Abrams, D., Ellis, S., Sporton, S.C., Schilling, R.J.: Validation of Three-Dimensional Cardiac Image Integration: Use of Integrated CT Image into Electroanatomic Mapping System to Perform Catheter Ablation of Atrial Fibrillation. Journal of Cardiovascular Electrophysiology **17**(4) (April 2006) 341–348
8. Kistler, P.M., Rajappan, K., Harris, S., Earley, M.J., Richmond, L., Sporton, S.C., Schilling, R.J.: The impact of image integration on catheter ablation of atrial fibrillation using electroanatomic mapping: a prospective randomized study. European Heart Journal **29**(24) (2008) 3029–3036
9. Daccarett, M., Segerson, N., Günther, J., Nölker, G., Gutleben, K., Brachmann, J., Marrouche, N.: Blinded correlation study of three-dimensional electro-anatomical image integration and phased array intra-cardiac echocardiography for left atrial mapping. Europace **9** (2007) 923–926
10. Ector, J., De Buck, S., Huybrechts, W., Nuyens, D., Dymarkowski, S., Bogaert, J., Maes, F., Heidbüchel, H.: Biplane three-dimensional augmented fluoroscopy as single navigation tool for ablation of atrial fibrillation: Accuracy and clinical value. Heart Rhythm **5**(7) (March 2008) 957–964
11. Sra, J., Narayan, G., Krum, D., Malloy, A., Cooley, R., Bhatia, A., Dhala, A., Blanck, Z., Nangia, V., Akhtar, M.: Computed Tomography-Fluoroscopy Image Integration-Guided Catheter Ablation of Atrial Fibrillation. J Cardiovasc Electrophysiol **18**(4) (April 2007) 409–414
12. De Buck, S., Maes, F., Ector, J., Bogaert, J., Dymarkowski, S., Heidbüchel, H., Suetens, P.: An Augmented Reality System for Patient-Specific Guidance of Cardiac Catheter Ablation Procedures. IEEE Transactions on Medical Imaging **24**(11) (November 2005) 1512–1524
13. Brost, A., Liao, R., Hornegger, J., Strobel, N.: 3-D Respiratory Motion Compensation during EP Procedures by Image-Based 3-D Lasso Catheter Model Generation and Tracking. In: Lect. Notes Comput. Sci. Volume 5761., London (2009) 394–401
14. Brost, A., Wimmer, A., Liao, R., Hornegger, J., Strobel, N.: Catheter Tracking: Filter-Based vs. Learning-Based. In Goesele, M., Roth, S., Kuijper, A., Schiele, B., Schindler, K., eds.: Pattern Recognition. Volume 6376 of Lecture Notes in Computer Science. Springer Berlin / Heidelberg (2010) 293–302
15. Brost, A., Liao, R., Hornegger, J., Strobel, N.: Model-Based Registration for Motion Compensation during EP Ablation Procedures. In Fischer, B., Dawant, B., Lorenz, C., eds.: Biomedical Image Registration. Volume 6204 of Lecture Notes in Computer Science. Springer Berlin / Heidelberg (2010) 234–245
16. Brost, A., Liao, R., Strobel, N., Hornegger, J.: Respiratory motion compensation by model-based catheter tracking during EP procedures. Medical Image Analysis **14**(5) (2010) 695–706 Special Issue on the 12th International Conference on Medical Image Computing and Computer-Assisted Intervention (MICCAI) 2009.
17. Quan, L.: Conic Reconstruction and Correspondence From Two Views. IEEE Trans Pattern Anal Mach Intell **18**(2) (February 1996) 151–160
18. Cychosz, J.: Efficient Binary Image Thinning using Neighborhood Maps. Graphics Gems IV (1994) 465–473

19. Breu, H., Gil, J., Kirkpatrick, D., Werman, M.: Linear time Euclidean distance transform algorithms. IEEE Trans Pattern Anal Mach Intell **17** (May 1995) 529–533
20. Viola, P., Jones, M.: Robust real-time face detection. Int. J. Comput. Vision **57**(2) (2004) 137–154
21. Freund, Y., Schapire, R.: A decision-theoretic generalization of on-line learning and an application to boosting. JCSS **55**(1) (1997) 119–139
22. Breiman, L., Friedman, J., Olshen, R., Stone, C.: Classification and Regression Trees. Chapman & Hall, New York, USA (1984)
23. Ector, J., De Buck, S., Loeckx, D., Coudyzer, W., Maes, F., Dymarkowski, S., Bogaert, J., Heidbüchel, H.: Changes in left atrial anatomy due to respiration: Impact on three-dimensional image integration during atrial fibrillation ablation. J Cardiovasc Electrophysiol. **19**(8) (August 2008) 828–834
24. Gepstein, L., Hayam, G., Ben-Haim, S.: A Novel Method for Nonfluoroscopic Catheter-Based Electroanatomical Mapping of the Heart: In Vitro and In Vivo Accuracy Results. Circulation **95** (1997) 1611–1622